Potential of membrane distillation in seawater desalination: Thermal efficiency, sensitivity study and cost estimation

Sulaiman Al-Obaidani [a,b,*], Efrem Curcio [b,c], Francesca Macedonio [b], Gianluca Di Profio [b], Hilal Al-Hinai [d], Enrico Drioli [b,c]

[a] Department of Mechanical and Industrial Engineering, Sultan Qaboos University, P.O. Box 33 Al-Khod, P.C. 123, Oman
[b] Department of Chemical Engineering and Materials, University of Calabria, Via P. Bucci Cubo 44/A, 87030 Rende, CS, Italy
[c] Institute on Membrane Technology ITM-CNR, Via P. Bucci Cubo 17/C, 87030 Rende, CS, Italy
[d] The Research Council, P.O. Box 1422, P.C. 130, Al-Athaiba – Muscat, Oman

ARTICLE INFO

ABSTRACT

In this work, an extensive analysis on direct contact membrane distillation (DCMD) performance was developed to estimate the mass flux and the heat efficiency, considering transport phenomena, membrane structural properties and most sensitive process parameters, with the aim to provide optimization guidelines for materials and methods. The results showed that an increase of the temperature gradient resulted in the enhancement of both transmembrane flux and thermal efficiency. The investigation of the effects of membrane properties confirmed that better DCMD performance was achieved when using polymeric membranes characterized by low thermal conductivity (flux and thermal efficiency declined by 26% and 50%, respectively, when increasing thermal conductivity from 0.1 to 0.5 W/m K), and high porosity. An optimal thickness value (around 0.7 mm) was identified when operating at low temperature gradient (<5 °C). However, at higher temperature gradient (>10 °C), increasing the membrane thickness from 0.25 to 1.55 mm resulted in a flux decay of about 70% without a significant improvement in thermal efficiency.

Exergy analysis, sensitivity study and economical evaluation were carried out to assess the feasibility of DCMD process. For DCMD with heat recovery, the estimated water cost was $1.17 m^{-3}, which was comparable to the cost of water produced by conventional thermal processes: i.e. around $1.00 m^{-3} for multiple effect distillation (MED) and $1.40 m^{-3} for multi-stage flash (MSF). However, significant savings are expected when using a low-grade thermal energy source, decreasing the cost of DCMD to values approaching the cost of water produced by reverse osmosis (RO), which is about $0.50 m^{-3}.

© 2008 Elsevier B.V. All rights reserved.

1. Introduction

Membrane distillation (MD) is a thermal membrane separation process that involves transport of vapor through microporous hydrophobic membranes and operates on the principle of vapor–liquid equilibrium as a basis for molecular separation. The driving force of the process is supplied by the vapor pressure difference caused by temperature gradient imposed between the liquid–vapor interfaces. MD has potential applications in many areas of scientific and industrial interest, yielding highly purified permeate and separating contaminants from liquid solutions. It has been tested in the treatment of thermally sensitive industrial products such as concentrating aqueous solution in fruit juices [1], in pharmaceutical industry [2], in wastewater treatment [3] and water desalination [4–7].

In particular, the MD process can be used as a substitute for conventional desalination processes such as multi-stage flash (MSF), reverse osmosis (RO), and multiple effect distillation (MED). The advantages of MD compared to these processes are as follows: (i) lower operating temperatures and vapor space required than MSF and MED, (ii) lower operating pressure than RO, (iii) 100% (theoretical) rejection of non-volatile solute, and (iv) performance not limited by high osmotic pressure or concentration polarization.

Recently, the interest of using MD process for desalination is increasing worldwide due to these attractive features, especially when coupled with solar energy or utilizing low-grade heat source [8–10].

In 2004, researchers at the University of Texas at El Paso (UTEP) in collaboration with the Swedish firm SCARAB DEVELOPMENT AB [11] investigated methods coupling solar pond technology with

* Corresponding author at: Department of Chemical Engineering and Materials, University of Calabria, Via P. Bucci Cubo 44/A, 87030 Rende, CS, Italy.
Tel.: +39 0984492012; fax: +39 0984492103.
E-mail address: sobeidani@squ.edu.om (S. Al-Obaidani).

desalination to create a zero discharge system, and MD was one of the technologies that was investigated as part of the zero discharge concept [12].

In addition, coupling MD with solar energy is the basic concept of the MEDESOL (seawater desalination by innovative solar-powered membrane distillation system) project, aiming to develop an environmentally friendly desalination technology for fresh water supply in arid and semi-arid regions. The layout involves the concept of multi-step MD, to be implemented in the solar platform of Almeria (Spain), in order to minimize specific energy and membrane area required [13].

The SMAll-scale, stand alone DEsalination System (SMADES system), realized under the namesake EU funded project, and was designed to provide potable water in remote coastal areas with low infrastructure and without connection to a grid. The desalination units were based on MD modules with internal heat recovery function; the required energy was supplied by solar thermal collectors in the form of heat on a temperature level of 60–80 °C with 72 m² of collector area and a solar heat storage water tank of 3 m³. The electrical auxiliary energy required to drive the pumps and valves was supplied by photovoltage (PV) panels [14].

Memstill® is a newly developed membrane-based distillation concept, claimed to have the potential to improve the economy and ecology of existing desalination technologies for seawater and brackish water to a large extent. This technology combined MSF and MED modes into one air gap membrane distillation module. The process promised to decrease desalination costs to $0.26 m⁻³, using low-grade waste steam or heat as driving force [15]. For comparison, the unit cost of water produced by conventional thermal desalination is around $1.00 m⁻³ for MED and $1.40 m⁻³ for MSF [16], while it is around $0.5 m⁻³ for RO [17].

The integration of direct contact membrane distillation (DCMD) and/or solar-powered vacuum membrane distillation with conventional pressure-driven membrane operations (such as MF, UF; NF, RO, MBR) is one of the key issues of the EU-funded MED-INA (MEmbrane Desalination Systems: an INtegrated Approach) project, implemented by a consortium of 14 partners, aimed to limit the brine disposal problem and to drastically enhance the water recovery factor [18].

The MD system to be considered in our study is the one in which the liquid phases are in direct contact with both sides of the membrane (DCMD) as shown in Fig. 1a. Among the other MD configurations [19], characterized by the way by which the vapor is recovered in the permeate side, DCMD is simplest to operate – does not require vacuum pump as in vacuum membrane distillation (VMD), nor condenser as in sweep gas membrane distillation (SGMD) or cooling surface as in air gap membrane distillation (AGMD) – and the distillation process can be carried out in any desired membrane configuration (flat sheet, spiral wound, capillaries or hollow fibers). Thus, DCMD can be conveniently applied for investigations in which water is the major fluxing component, such as in desalination [20–23].

The necessity to select carefully the physico-chemical properties of the MD membranes in order to ensure a high process efficiency is today accepted [5]; on the other hand, it is recognized that there are no membranes in the market specifically manufactured and optimized to be used for MD desalination processes. Since more than 20 years, the available hardware for MD processes consists of microporous hydrophobic membranes (usually made in polypropylene (PP), polyvinylidenefluoride (PVDF) or polytetrafluoroethylene (PTFE)) normally designed for pressure-driven filtration processes rather than for concentration/temperature-driven mass transfer. Only few specific examples exist for concentration-driven mass transfer, such as the Liqui-Cel module offered by CELGARD LLC (with fibers in PP for gas/liquid mass transfer or osmotic membrane

distillation, but not applicable for MD purposes); the modules with capillary PP membranes provided by Microdyn-Nadir GmbH; the DISSO₃LVE™ module with fibers in PTFE commercialized by WL Gore & Associates; the flat sheets PVDF membranes commercialized by GVS [24].

This study is aiming to assign some criteria for the optimization of the membrane properties (such as thickness, porosity, tortuosity and thermal conductivity coefficient) in order to increase the performance of MD unit with respect to both transmembrane flux and thermal efficiency. In addition, exergy analysis, economic evaluation and sensitivity analysis were conducted to assess the feasibility of MD as desalination process.

1.1. Theoretical background

1.1.1. Correction for shell side flow distribution

Hollow fiber contactors are compact devices offering high interfacial area for the contact of fluid phases with membrane. Membrane contactors have been demonstrated in a diverse range of gas/liquid and liquid/liquid applications; for DCMD, the diffusive mass transfer across the membrane is typically obtained by flowing the heated feed solution through the lumen side, and the cooled permeate through the shell side of the module.

In most cases, fibers are not arranged in an ordered way inside a module and they are not distributed uniformly on the shell side especially when existing in large number. As a result, hollow fiber modules often exhibit a flow maldistribution that decreases their performance in terms of mass and energy transfer. Voronoi tessellation method was used to evaluate the flow distribution in the shell of a randomly packed hollow fiber module [25]. Voronoi tessellation is a mathematical method able to model the geometric characteristics of random spacing of different objects; according to this approach, the space between randomly packed objects is subdivided by drawing straight boundaries equidistant between neighbouring objects, forming polygonal cells. In details, the cross-section area was subdivided into polygonal cells, each one associated to a single fiber. The probability density distribution function $f(\varphi)$ of polygonal cell area is [26]:

$$f(\varphi) = \frac{s^s}{\bar{\varphi}^s} \frac{\varphi^{s-1}}{(s-1)!} \; e^{-s\varphi/\bar{\varphi}} \tag{1.a}$$

$$\varphi = a - a_f \tag{1.b}$$

$$\bar{\varphi} = a_0 - \bar{a}_f \tag{1.c}$$

$$a_0 = \frac{\pi R_M^2}{N_f} \tag{1.d}$$

$$\phi = \frac{\bar{a}_f}{a_0} \tag{1.e}$$

where s is the number of nearest neighbour fibers, was assumed equal to 4 and 6 at low (<0.6) and high (>0.6) packing density, respectively. The probability $\varXi$ that a polygonal cell has a packing fraction between ϕ_1 and ϕ_2 is [27]:

$$\varXi = \int_{\xi_1}^{\xi_2} s^s \frac{\xi^s}{(s-1)!} \; e^{-s\xi} \, d\xi \tag{2.a}$$

$$\xi_i = \frac{(1-\phi_i)\phi}{(1-\phi)\phi_i}, \quad i = 1, 2 \tag{2.b}$$

The effective flow distribution in the overall fiber bundles has been evaluated in term of the product of the friction factor (f) and the Reynolds number (Re). Assuming that the pressure drop in all the
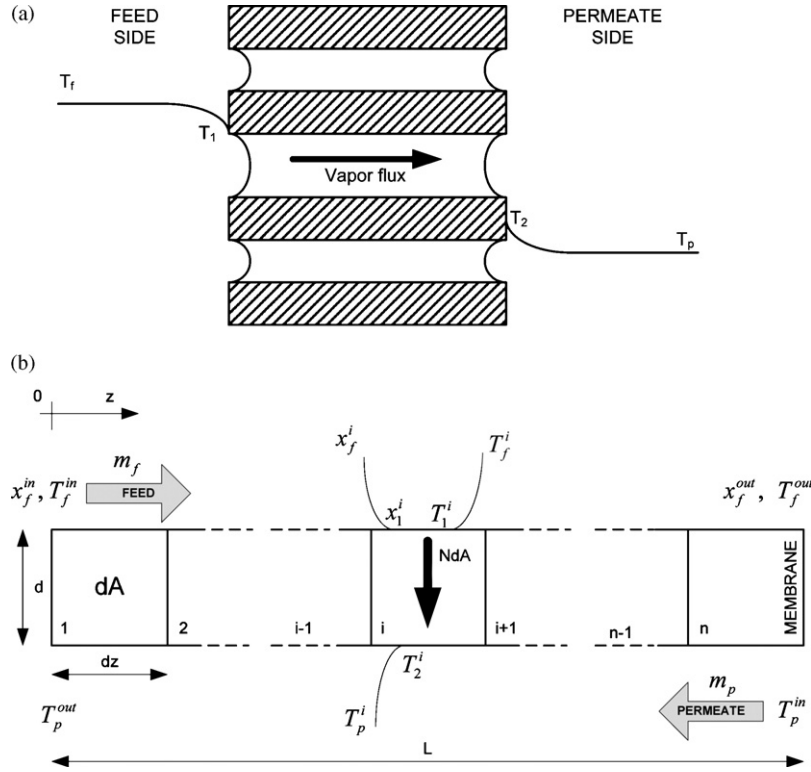
Fig. 1. (a) Concept of direct contact membrane distillation and (b) schematic representation of the DCMD modeling procedure.

cells is identical, and that the total mass flow rate is equal to the sum of the individual cell mass flow rate, the effective $(fRe)_e$ is given by

$$\frac{1}{(fRe)_e} = \sum_{i=1}^{m} \frac{1}{(fRe)_i} \left[\frac{(1-\phi_i)\phi}{(1-\phi)\phi_i} \right]^3 P_i \qquad (3)$$

where $(fRe)_i$ and P_i are estimated for the ith category.

1.1.2. Mass and heat transfer in DCMD

MD involves mass transfer of water vapor through a microporous membrane, coupled with heat transfer across the membrane and through the boundary layers adjacent to the membrane surfaces.

The average pore diameter of the membranes investigated was 0.2 μm, and thus comparable to the mean free path of water vapor molecules (0.11 μm at 60 °C) [28]. Therefore, the reduced Knudsen-molecular diffusion transition form of the dusty-gas model (DGM) was applied for describing the vapor flux of pure water across the membrane [19]:

$$N = -\frac{1}{RT_{avg}} \left(\frac{D_w^k D_{w-a}^0}{D_{w-a}^0 + p_a D_w^k} \right) \frac{\Delta p}{\delta} M \qquad (4.a)$$

with

$$D_w^k = \frac{2\varepsilon r}{3\tau} \sqrt{\frac{8RT_{avg}}{\pi M}} \qquad (4.b)$$

and

$$D_{w-a}^0 = 4.46 \times 10^{-6} \frac{\varepsilon}{\tau} T_{avg}^{2.334} \qquad (4.c)$$

where Δp is the partial pressure gradient of water through both membrane surfaces generated by a temperature gradient and/or a concentration difference, is the driving force to mass transfer in DCMD.

The heat transfer equations governing heat flows in and around the membrane are as follows:

- along the module at feed and permeate sides:

$$dQ_f = c_{pf}(\dot{m}_f - N\,dA)\,dT_f \qquad (5.a)$$

$$dQ_p = c_{pp}(\dot{m}_p - N\,dA)\,dT_p \qquad (5.b)$$

- within the boundary layers at feed and permeate sides:

$$dQ_f = h_f(T_f - T_1)\,dA \qquad (6.a)$$

$$dQ_p = h_p(T_2 - T_p)\,dA \qquad (6.b)$$

- across the membrane:

$$dQ_m = \left[N\lambda + \frac{k_m}{\delta}(T_1 - T_2) \right]\,dA \qquad (7)$$

- overall heat balance at the steady state:

$$dQ_f = dQ_m = dQ_p \qquad (8)$$

The conduction heat transfer coefficient k_m was estimated from vapor and solid phase thermal conductivities as

$$k_m = (1-\varepsilon)k_s + \varepsilon k_v \qquad (9)$$

where k_s is generally one order of magnitude greater than k_v [19].

Interfacial temperatures T_1 and T_2 were analytically obtained by solving Eqs. (6.a), (6.b), (7) and (8):

$$T_1 = \frac{\alpha(T_p + \beta T_f) + h_f T_f - N\lambda}{\alpha + h_f + \alpha\beta} \qquad (10.a)$$

$$T_2 = \frac{\alpha(T_f + \beta^{-1} T_p) + h_p T_p + N\lambda}{\alpha + h_p + \alpha\beta^{-1}} \qquad (10.b)$$

with $\alpha = (k_m/\delta)$ and $\beta = (h_f/h_p)$.

Concentration polarization phenomenon, related to the increase of the feed concentration in proximity of the membrane surface due to the retained solute, was evaluated by

$$\frac{x_1}{x_f} = e^{N/k_x \rho} \tag{11}$$

The temperature and the concentration of the solution vary in the axial direction along the module; variations in the bulk were obtained by solving the heat and mass balance equations for each differential element in which a membrane module is supposed to be divided (as schematised in Fig. 1b):

$$\frac{dT_f}{dz} = \frac{[N\lambda + \alpha(T_1 - T_2)]N_f \pi d_{m,ln}}{\dot{m}_f c_{pf}} \tag{12.a}$$

$$\frac{dT_p}{dz} = \frac{[N\lambda + \alpha(T_1 - T_2)]N_f \pi d_{m,ln}}{\dot{m}_p c_{pp}} \tag{12.b}$$

Differential Eqs. (12.a) and (12.b) were solved with the following boundary conditions:

$$T_f = T_f^{in} \quad \text{at } z = 0 \tag{13.a}$$

$$T_p = T_p^{out} \quad \text{at } z = L \tag{13.b}$$

The increase of feed concentration alongside the module was calculated as

$$dx_f = \frac{NdA(1 - x_f)}{\dot{m}_f - NdA} \tag{14}$$

assuming the boundary condition:

$$x_f = x_f^{in} \quad \text{at } z = L \tag{15}$$

The heat lost to the surroundings was assumed negligible for two main reasons: (i) the housings of the membrane modules used in this research were made of PVC, a thermal-insulator material with low thermal conductivity ($\sim$0.2 W/m K) and (ii) the cold permeate stream was recirculated in the shell side.

The overall heat flux in the DCMD process, expressed in terms of the global heat transfer coefficient H, was calculated as [29]:

$$Q_{tot} = H(T_f - T_p) = \left(\frac{1}{h_f} + \frac{1}{(k_m/\delta) + (N\lambda/(T_1 - T_2))} + \frac{1}{h_p} \right)^{-1}$$
$$\times (T_f - T_p) \tag{16}$$

The thermal efficiency of the DCMD process, defined as the ratio of the vaporization heat associated with the transmembrane water flux over the total heat flux, was expressed as

$$\eta \ (\%) = \frac{N\lambda}{\left(\frac{1}{h_f} + \frac{1}{(k_m/\delta)+(N\lambda/(T_1-T_2))} + \frac{1}{h_p} \right)^{-1} (T_f - T_p)} \times 100 \tag{17}$$

Eqs. (4), (10) and (12) show the complex relationships between heat and mass transfer existing in DCMD; calculating mass and energy fluxes follows an iterative scheme to be solved by computational procedures.

1.1.3. Simulation procedure

Physico-chemical properties of water and concentrated salt solutions were obtained from [30,31]. As a first step, morphological parameters (average pore size, porosity, tortuosity and thickness), physical properties of membranes (thermal conductivity), and geometrical parameters of modules (number of fibers, packing factor, hydraulic diameter and flow-channel length) as well as DCMD operating conditions (temperatures and flow rates of feed and permeate streams) were defined.

The DCMD module was subdivided into n differential elements as shown in Fig. 1b. The differential mass and heat balance equations were written for each differential element and they were solved by numerical fourth order Runge–Kutta method. In order to solve the system of ordinary differential equations (12.a), (12.b) and (14) with splitting boundary values, a shooting method has been employed. While the boundary condition (13.a) and (15) were applied, the permeate temperature at $z = 0$ (T_p^{out}) was supposed. For each ith differential element, the interfacial temperatures T_1^i and T_2^i were assumed – as an initial guess – equal to feed and permeate bulk temperatures T_f^i and T_p^i, respectively. Analogously, the interfacial concentration x_f^i was assumed – as an initial guess – equal to feed bulk concentration x_f. Effective values of Reynolds number, evaluated for non-uniform module packing fractions, were used in the calculation of mass and heat transfer coefficients. The vapor flux and the corresponding temperature and concentration distributions for each ith differential element were computed iteratively using the method of successive substitution until the difference between two consecutive iterations was less than 0.1%. Then, the solution was marched forward until $z = L$, and then the guessed value of T_p^{out} was adjusted by secant method; this procedure was repeated until the boundary condition in (13.b) was met within an error of 0.1%.

The algorithm was implemented in Matlab version 7.0.1 (R14). For a single differential element, the mass and heat transfer coefficients on both feed and permeate sides were evaluated using suitable empirical correlations provided by literature [19]. The vapor pressure was calculated using Antoine equation and corrected by the activity coefficient as shown in Appendices A1 and A2 which give the method used to calculate vapor pressure and water activity.

2. Experimental

The flow chart of the experimental apparatus used for DCMD tests is shown in Fig. 2. Feed and distillate streams were driven by CASTER MT7002PP pumps (A), and flow rates measured by BROOKS INSTRUMENTS flow-meters (B). A thermostatic bath Digital Plus NESLAB RTE17 (C) and an ISCO GTR 2000 heater (D) provided, at the inlet of the module, the maintenance of distillate and feed temperatures, respectively. A REFLEX HP 8200 balance (E) connected to the distillate tank has been used to estimate the transmembrane solvent flux by measuring the weight variations ($\pm$0.1 g) over time. Temperatures were monitored by SPER SCIENTIFIC 800012 Pt thermocouples (*T*) with sensitivity $\pm$0.1 °C.

The system was operated in a counter-current flow configuration with the feed solution flowing inside the fibers and the permeate solution on the shell side of the membrane module.

Validation experiments were performed using four different modules (specifications listed in Table 1) in order to confirm the general validity of the simulation model.

Feed solutions for DCMD tests were aqueous NaCl solutions at concentration of 35 g/L (TDS of standard seawater).

3. Results and discussion

3.1. Correction for randomly packed hollow fiber bundles

The fluid maldistribution in the shell side due to a non-uniform packing of the fibers is mathematically quantified by the cumulative probability distribution reported in Fig. 3, generated by Eqs. (2.a) and (2.b). The diagram shows that, for a global packing fraction of 0.7 (i.e.: MD020CP2N module), the cross-section area at the shell side with local packing fractions comprised within the range
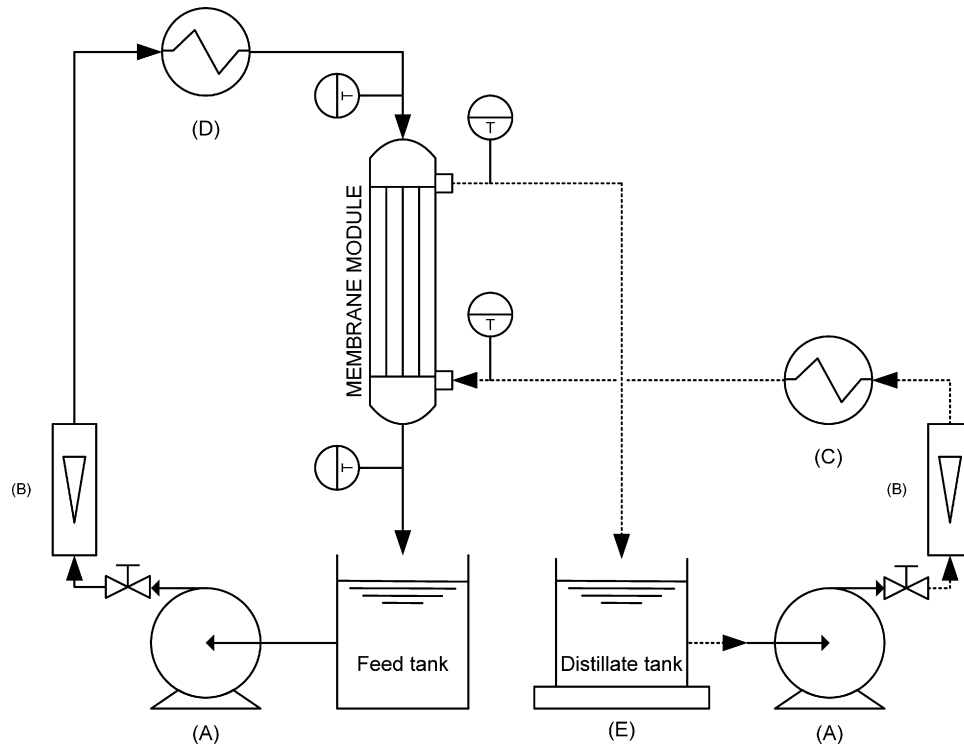
Fig. 2. Scheme of the experimental DCMD apparatus: (A) circulation pump; (B) flowmeters; (C) thermostatic bath; (D) heater; (E) balance; (T) thermocouples. Solid line: feed stream; dotted line: distillate stream.

$0.7 \pm 10\%$ represents the 56% of the total cross-section area of the module. On the other hand, at lower global packing fraction (i.e.: MD080CO2N module), the cross-section area at the shell side with local packing fractions comprised between $0.5 \pm 10\%$ decreased to 27% of the total cross-section area of the module, so exacerbating the negative effects of the flow maldistribution.

As shown in Fig. 4, the non-uniform distribution of the hollow fiber bundles has a detrimental effect on the fluid-dynamics of the contactor, whose performance (described in terms of fRe, as from Eq. (3)) approaches ideality at increasing packing fraction. Mass and heat transfer coefficients at the shell side are therefore improved at higher packing fractions, in agreement the well-known behavior of tube-and-shell heat exchangers [30]. In particular, the ratio $(fRe)_e/(fRe)_{id}$ increased from 0.26 to 0.69 when the global packing fraction of the module increased from 0.15 to 0.7.

The consequent benefits in terms of transmembrane flux can be deduced from simulation data reported in Table 2, showing that the MD080CO2N module exhibits a flux 28% lower with respect to MD020CP2N module, although both of them are manufactured using the same kind of fibers but with different lengths, which might slightly contribute to a reduction in flux for the longer module ($T_f^{in} = 55\,^{\circ}C$, $T_p^{in} = 25\,^{\circ}C$). Zhongwei et al. [27] have found that fluxes differ by 25% between modules with packing fractions of 0.5 and 0.7 ($T_f^{in} - T_p^{in} = 45\,^{\circ}C$).

3.2. Effects of the operating conditions

In order to prove the validity of the DCMD model, the predicted values of transmembrane flux were compared with experimental results obtained using four different modules. Flux measurements were carried out by keeping the temperature at the permeate side constant at $15\,^{\circ}C$ and the mass flow rate was kept at 0.055 kg/s at feed side and 0.028 kg/s at permeate side for all modules. As shown in Fig. 5a, when the feed side temperature was increased from 25 to $70\,^{\circ}C$, the flux was increasing exponentially as a consequence of the increase in the thermal driving force, as

Table 1
DCMD modules characteristics and membrane properties

	MD020CP2N	MD080CO2N	Home-made	MD020TP2N
Manufacturer	Microdyn	Enka-Microdyn	–	Enka-Microdyn
Membrane material	Polypropylene	Polypropylene	Polypropylene	Polypropylene
Pore size (μm)	0.2	0.2	0.2	0.2
Fiber outer diameter (mm)	2.8	2.8	0.3	8.6
Fiber inner diameter (mm)	1.5	1.5	0.2	5.5
Membrane thickness (mm)	0.65	0.65	0.05	1.55
Number of fibers	40	467	1500	3
Shell inner diameter (m)	0.021	0.085	0.03	0.021
Packing factor	0.7	0.5	0.15	0.5
Length (m)	0.45	1.0	0.24	0.75
Surface area (m^2)	0.1	2	0.35	0.036
Porosity	0.7	0.7	0.45	0.7
Tortuosity[a]	1.4	1.4	2.2	1.4

[a] Assumed as $1/\varepsilon$ [32].

Table 2
Flux and temperature profiles alongside MD020CP2N and MD080CO2N modules

MD020CP2N[a]				MD080CO2N[b]			
Cumulative length (cm)	N (kg/m^2 h)	T_f (°C)	T_p (°C)	Cumulative length (cm)	N (kg/m^2 h)	T_f (°C)	T_p (°C)
0		**55.00**	30.00	0		**55.00**	32.00
2.25	5.55	55.00	30.00	5.00	4.11	55.00	32.00
4.50	5.48	54.72	29.72	10.00	4.05	54.61	31.60
6.75	5.42	54.44	29.44	15.00	3.98	54.22	31.21
9.00	5.35	54.16	29.16	20.00	3.92	53.83	30.82
11.25	5.29	53.89	28.89	25.00	3.86	53.45	30.44
13.50	5.23	53.61	28.61	30.0	3.80	53.07	30.07
15.75	5.17	53.34	28.34	35.00	3.74	52.70	29.69
18.00	5.11	53.07	28.07	40.00	3.68	52.34	29.32
20.25	5.05	52.80	27.80	45.00	3.63	51.97	28.96
22.50	4.99	52.53	27.53	50.00	3.57	51.61	28.60
24.75	4.93	52.27	27.27	55.00	3.52	51.26	28.24
27.00	4.88	52.01	27.01	60.00	3.47	50.91	27.89
29.25	4.82	51.74	26.74	65.00	3.42	50.56	27.54
31.50	4.77	51.48	26.48	70.00	3.37	50.22	27.20
33.75	4.71	51.22	26.22	75.00	3.32	49.88	26.86
36.00	4.66	50.97	25.97	80.00	3.27	49.54	26.52
38.25	4.60	50.71	25.71	85.00	3.22	49.21	26.18
40.50	4.55	50.46	25.46	90.00	3.18	48.88	25.85
42.75	4.50	50.21	25.21	95.00	3.13	48.56	25.53
45.00	4.5	50.00	25.00	100.00	3.09	48.23	25.00

$T_f^{in} = 55$ °C, $T_p^{in} = 25$ °C, $Re = 900$ at feed side, ideal $Re = 500$ at permeate side.
[a] Average flux: 4.98.
[b] Average flux: 3.57.

predicted by the Clausius–Clapeyron equation (Eq. (A.1)) which describes the dependence of water vapor pressure on temperature.

The simulation results reported in Fig. 5b confirmed that the thermal efficiency significantly enhanced at higher feed temperatures: for instance, it improved by 35%, 32%, and 6% for MD020CP2N, MD020TP2N and home-made modules, respectively, when feed temperature increased from 25 to 70 °C. The thermal efficiency of MD080CO2N module improved by 14% when feed temperatures increased from 25 to 55 °C.

Additionally, the transmembrane flux and thermal efficiency can be enhanced by increasing the feed flow rate, i.e. improving the hydrodynamic conditions in terms of Reynolds number, mass

and heat transfer coefficients. Fig. 6a shows the results of two sets of experiments conducted on the MD020CP2N module at feed temperatures of 40 and 60 °C; the feed flow velocity was increased from 0.2 to 1.0 m/s, while the permeate flow velocity and temperature were kept constant at 0.28 m/s and 15 °C, respectively.

The results showed that the flux was increased by 24 and 38% at feed temperatures of 40 and 60 °C, respectively. Curves of Fig. 6a tend to reach a plateau; at this point, an increase in feed velocity does not lead to significant benefits in terms of transmembrane flux. Therefore, it is possible to set a recommended fluid velocity through hollow fibers – in laminar regime – that ranges within 0.9–1.0 m/s, corresponding for MD020CP2N module (the most efficient among the four modules tested) to Reynolds number around 1900.
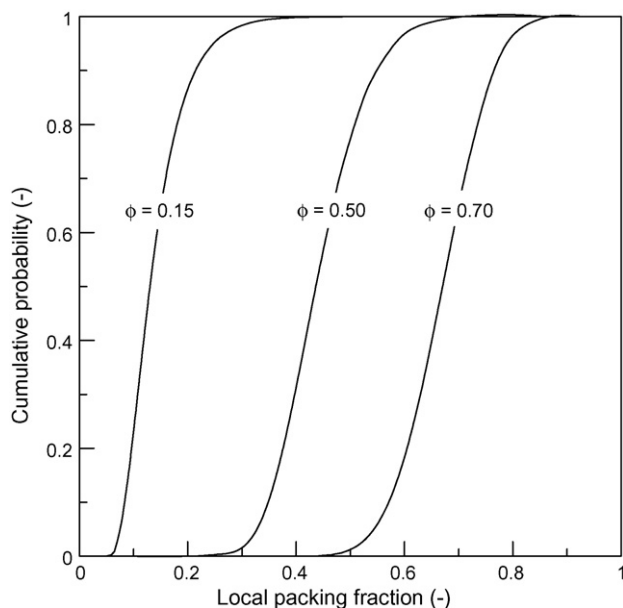
Fig. 3. Cumulative probability distribution vs. local packing fraction for different packing densities.
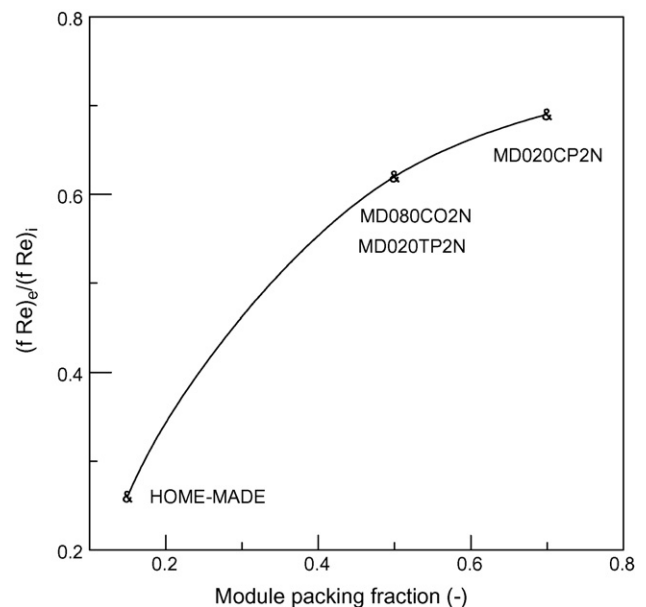
Fig. 4. Effect of the non-uniform packing of fibers on the fluid-dynamics of different DCMD modules.

There was slight enhancement in the thermal efficiency since it increased by 2% and 5% at feed temperature of 40 and 60 °C, respectively, as reported in Fig. 6b.

The DCMD performance with solution concentration ranging from 35 to 350 g/L (saturated NaCl solution) is reported in Fig. 7
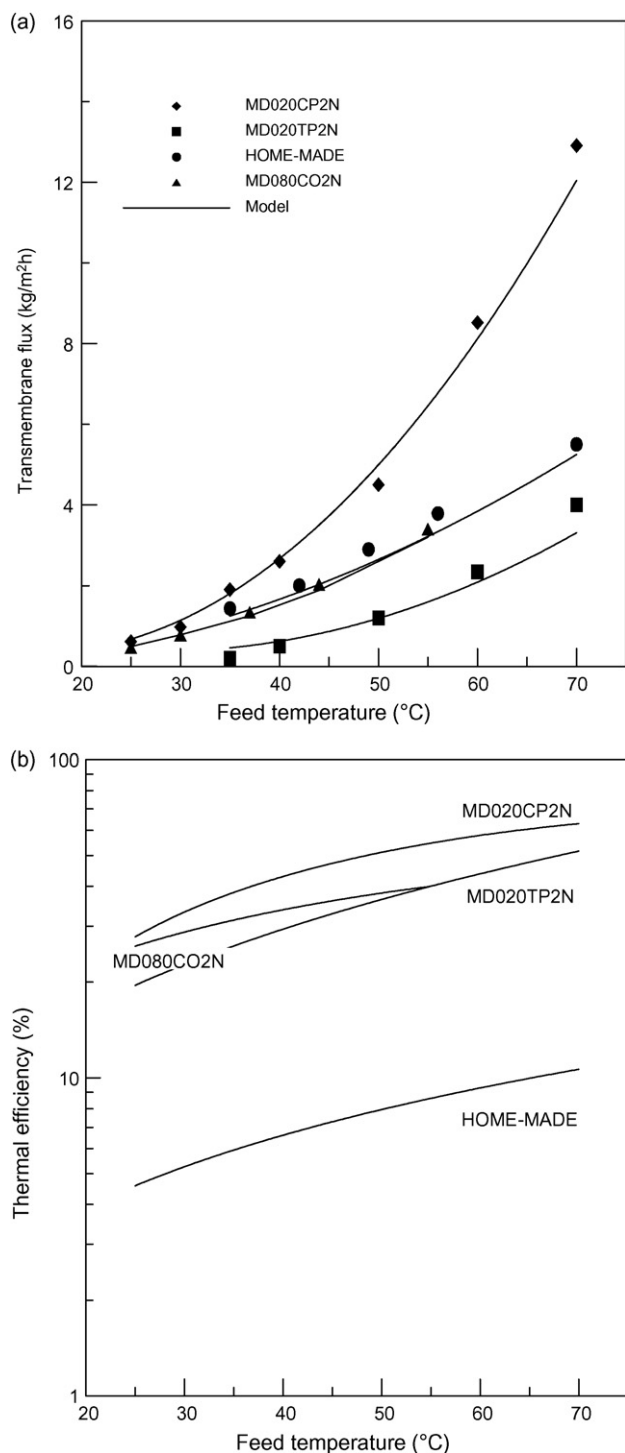
Fig. 5. (a) Experimental and simulation results showing the effects of the feed temperature on the DCMD flux for different membrane modules ($\dot{m}_f = 0.055$ kg/s, $\dot{m}_p = 0.027$ kg/s, $T_p^{in} = 15$ °C, feed concentration = 35 g/L) and (b) simulation results showing the effects of the feed temperature on the thermal efficiency of DCMD for different membrane modules ($\dot{m}_f = 0.055$ kg/s, $\dot{m}_p = 0.027$ kg/s, $T_p^{in} = 15$ °C, feed concentration = 35 g/L).
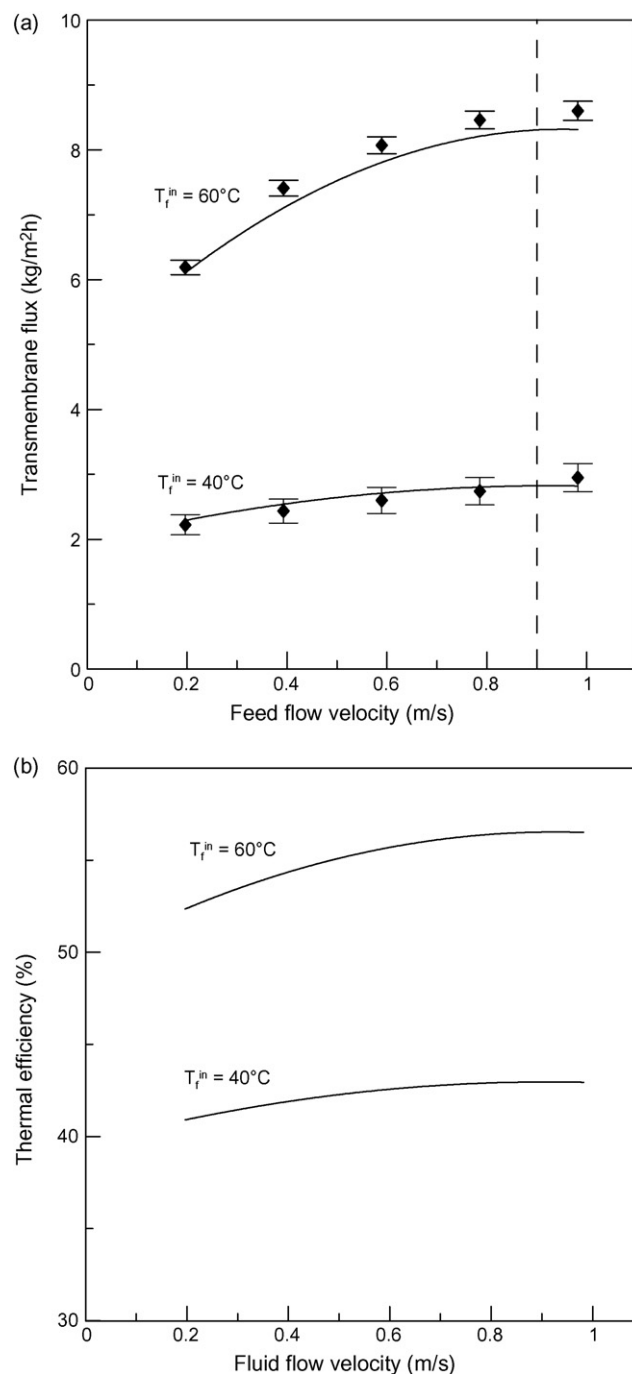
Fig. 6. (a) Experimental and simulation results showing the effects of the feed flow velocity on the DCMD flux ((MD020CP2N module, $v_p = 0.28$ m/s, $T_p^{in} = 15$ °C, feed concentration = 35 g/L) and (b) simulation results showing the effects of the feed flow velocity on the DCMD thermal efficiency (MD020CP2N module, $v_p = 0.28$ m/s, $T_p^{in} = 15$ °C, feed concentration = 35 g/L).

(MD020CP2N module, $T_f^{in} = 55$ °C; $T_p^{in} = 25$ °C; feed and permeate flow velocities set to 0.39 and 0.28 m/s, respectively).

The results showed that the MD transmembrane flux was decreasing slightly (by 5%) when the concentration increased from 35 to 75 g/L (a value close to typical RO brine composition). Since the driving force in DCMD process is a partial pressure difference, the transmembrane flux was not limited by the osmotic pressure; this fact allowed operation at high solution concentration ranges where RO normally fails. Therefore, MD seems an attractive
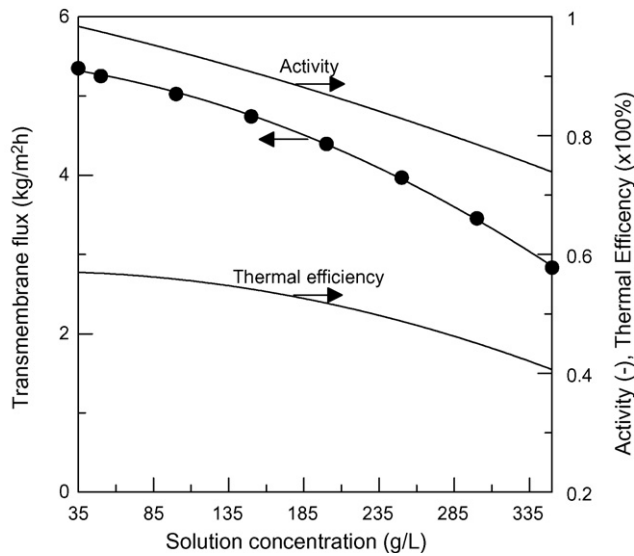
Fig. 7. Effect of the solution concentration on the DCMD performance (MD020CP2N module, feed flow velocity = 0.39 m/s, permeate flow velocity = 0.28 m/s, $T_f^{in} = 55$ °C; $T_p^{in} = 25$ °C). Points from experiments and lines from simulation.

Fig. 8. Simulation results of the effects of the membrane thermal conductivity on the DCMD performance ($v_f = 0.90$ m/s, $v_p = 0.28$ m/s, $T_f^{in} = 55$ °C, $\Delta T = 25$ °C, feed concentration = 35 g/L, based on MD020CP2N module as a reference for membrane properties with changing k for simulation).

technique for seawater desalination when integrated with RO in the logic of the zero liquid discharge concept. The total flux decay was about 50% when the feed concentration was increased from 35 to 350 g/L, mainly because of the reduction in the activity of the solution (see data reported in Table A.1 of Appendix A), that decreased from an initial value of about 0.99 down to 0.73 in proximity of the saturation level, as shown in Fig. 7.

The thermal efficiency was decreasing from 58% to 40% as the feed concentration was increased from 35 to 350 g/L due to the reduction in the vaporization heat associated with the transmembrane flux.

In general, the simulation model was capable to estimate the transmembrane flux with average errors not exceeding 5%; therefore, it was used as a reliable tool for describing the DCMD process performance at different operating conditions and different membrane physical properties.

3.3. Effects of the membrane physical properties

Basic membrane physical properties, namely thickness, thermal conductivity and porosity were considered in this study. The operating conditions were always kept constant at feed inlet temperature of 55 °C, temperature difference of 30 °C, feed flow velocity of 0.90 m/s, permeate flow velocity of 0.28 m/s and feed concentration of 35 g/L. The results are presented in Figs. 8–10.

At present, available polymeric materials for manufacturing hydrophobic membranes suitable for MD are, typically, PP, PVDF and PTFE. As shown in Fig. 8, membrane materials with high thermal conductivity result in the reduction of both transmembrane flux and thermal efficiency (by 26% and 55%, respectively, when the thermal conductivity of the membrane increased from 0.05 to 0.5 W/m K). Polymeric membrane materials with higher thermal conductivity offer a lower thermal resistance; therefore, the conduction heat transferred through the membrane increases (according to Eq. (7)), which in turn reduces the amount of vaporization heat and, ultimately, both flux and thermal efficiency.

In principle, the membrane surface should be made of material with small thermal conductivity; however, as shown in Fig. 8, for common hydrophobic polymers used in MD it is above 0.2 W/m K. Some materials exhibit thermal conductivities in the
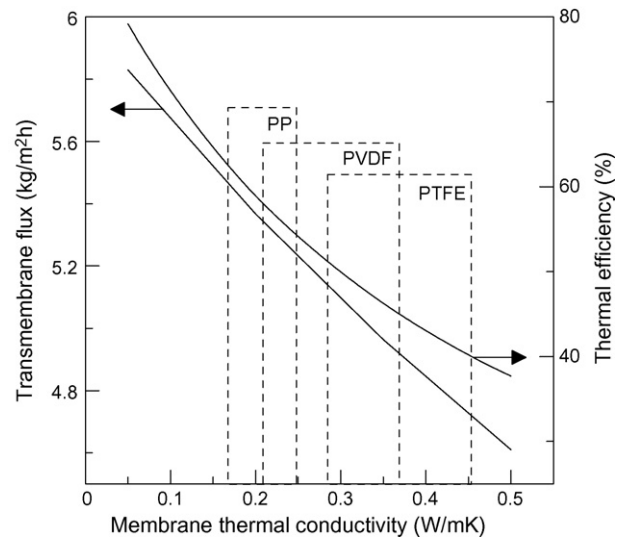
range of 0.13–0.18 W/m K (cellulose acetate and polyvinylchloride, polystyrene) and even less (polyurethane) [33]. In order to improve the performance of MD membranes, recent approaches consider the use of microporous hydrophobic/hydrophilic composite membrane, with a top hydrophobic thin layer responsible for the mass transport, and a hydrophilic sub-layer able to reduce the conductive heat loss through the whole membrane matrix. Specifically, they include: cellulose acetate or cellulose nitrate membranes modified via radiation graft polymerization of vinyltrimethyl-silicon/carbon tetrafluoride and octafluoro-cyclobutane [34], or surface modification of hydrophilic membranes by adding fluorinated surface-modifying macromolecules [35].

As shown in Fig. 9, the transmembrane flux declined rapidly when the membrane thickness was increased, as expected from the inverse proportional relationship between N and δ in Eq. (4.a). As a matter of fact, the flux dropped by about 70% when the membrane
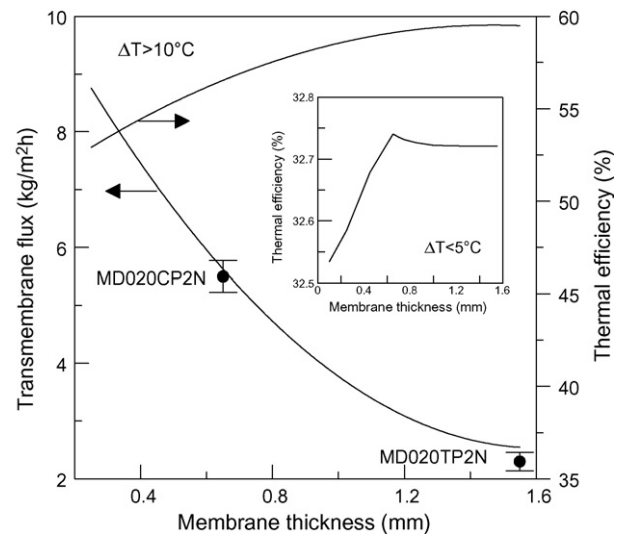
Fig. 9. Simulation and experimental results of the effects of the membrane thickness on the MD performance ($v_f = 0.90$ m/s, $v_p = 0.28$ m/s, $T_f^{in} = 55$ °C, $\Delta T = 25$ °C, feed concentration = 35 g/L, based on MD020CP2N module as a reference for membrane properties with changing δ for simulation).

thickness increased from 0.25 to 1.55 mm. However, a conflict exists between the requirements of high mass transfer associated with thinner membranes and low conductive heat losses achieved by using thicker membranes. In fact, the thermal efficiency increased gradually as the membrane thickness was increased when operating at temperature gradient higher than 10 °C. Therefore, the efficiency improved since the reduction in the heat conduction through the membrane (term k_m/δ in Eq. (17)) was always more significant than the decrease in the vaporization heat (term $N\lambda$ in Eq. (17)) due to flux decline occurring at higher membrane thickness. At low temperature difference (<5 °C), the thermal efficiency exhibited a maximum around 0.7 mm membrane thickness, as shown in the magnified scale in Fig. 9. In this case, the positive effect on the efficiency due to the reduction of k_m/δ is counterbalanced by the reduction of $N\lambda$, hence creating a plateau in the thermal efficiency profile.

Fig. 10 illustrates the effect of increasing membrane porosity on the DCMD performance. According to Eqs. (4.b) and (4.c), membranes with higher porosity have higher effective molecular diffusions, leading to a flux enhancement. In addition, a high void fraction of the polymeric matrix reduces the thermal conductivity of the membrane, as in Eq. (9) and, ultimately, decreases the efficiency loss associated with the conductive heat flux. The calculations showed that as the membrane porosity was increased by 15%, the vapor flux and the thermal efficiency for the MD020CP2N module ($\varepsilon = 0.70$) increased by 26% and 13%, respectively. A similar trend was found for the home-made module ($\varepsilon = 0.45$), whose vapor flux and thermal efficiency increased by 37% and 3%, respectively.

At present, typical porosity of commercial membranes used in MD operations are 0.7 for Accurel PP membranes (Mycrodyn), 0.75 for PVDF-made GVHP/HVHP membranes (Millipore) and 0.6 for TF series PTFE/PP-supported membranes [36].

3.4. Exergy analysis, sensitivity study and cost analysis

The exergy of a flow stream for a system in which the governing parameters are the temperature, the pressure and the composition, can be written as [37,38]:

$$Ex = Ex^{Temperature} + Ex^{Pressure} + Ex^{Concentration} \tag{18}$$
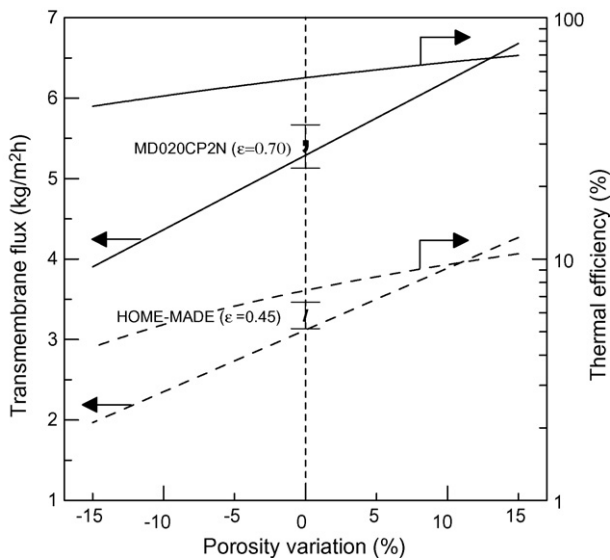
Fig. 10. Simulation and experimental results of the effects of the membrane porosity on the DCMD performance ($v_f = 0.90$ m/s, $v_p = 0.28$ m/s, $T_f^{in} = 55$ °C, $\Delta T = 25$ °C, feed concentration = 35 g/L, based on MD020CP2N module as a reference for membrane properties with changing ε for simulation).

Table 3
Summary of exergy analysis for DCMD plants with and without heat recovery (HR) system

	DCMD without HR	DCMD with HR
Ex^{out} (kW)	1,335	1,053
Ex^{in} (kW)	982	982
ΔEx (kW)	353	71
Work input (kW)	56	56
Heat input (kW)	45,036	39,690
Recovered heat (kW)	0	5,346
Exergy of work input (kW)	56	56
Exergy of heat input (kW)	4,180	3,684
Exergy of input streams (kW)	982	982
Total exergy input (kW)	5,218	4,722
Exergy output (kW)	1,335	1,335
Entropy production (kW)	3,883	3,669
Exergy efficiency (%)	25.6	28.3

$T_f^{in} = 55$ °C, $T_p^{in} = 25$ °C, water recovery 80%.

with

$$Ex^{Temperature} = \dot{m}c_p \left[(T - T_0) - T_0 \ln \left(\frac{T}{T_0} \right) \right] \tag{19}$$

$$Ex^{Pressure} = \dot{m} \left(\frac{P - P_0}{\rho} \right) \tag{20}$$

$$Ex^{Concentration} = -\dot{m}(n_{solv} \, RT_0 \ln x_{solv}) \tag{21}$$

The exergy efficiency ψ was used to evaluate the performance of a process and to compare it with conventional ones. It is defined as the ratio of the exergy output over the exergy input:

$$\psi = \frac{\sum Ex^{out}}{\sum Ex^{in}} \times 100 \tag{22}$$

The total irreversible entropy production ($R_s T_0$) is obtained by applying the energy balance according to the second law of thermodynamics as follows [39]:

$$R_s T_0 = Ex_{electrical} + Ex_{thermal} - \Delta Ex \tag{23}$$

where,

$$Ex_{electrical} = \frac{\dot{m} \, \Delta P}{1000 \eta_{pump}} \tag{24}$$

$$Ex_{thermal} = Q \left(\frac{1 - T_0}{T} \right) \tag{25}$$

$$\Delta Ex = \sum Ex^{in} + \sum Ex^{out} \tag{26}$$

Exergy calculations and economical evaluation were performed for a 24,000 m³/day DCMD desalination plant. Two case studies were considered in order to check the optimal performance: (1) DCMD operated without heat recovery (HR) system; (2) DCMD with HR system aiming to reuse the heat from the brine to preheat the feed seawater (heat recovery efficiency of 80%), as schematized in Fig. 11. A sample cost calculation is given in Appendix A3 and all calculations were based on recent economic data presented in Table A.2 obtained from field data and literature.

A summary of the exergy analysis for DCMD plants with and without HR system is presented in Table 3. The net exergy change between inlet and outlet streams was 71 kW in case of MD with HR and 353 kW in case of DCMD without HR.

The installation of the HR improved the exergy efficiency of the system since both the total exergy input and the total irreversible entropy production ($R_s T_0$) were 11.5% and 5.8% lower, respectively, for DCMD with HR. The exergy efficiency was 28.3% and 25.6% for MD with and without HR, respectively.
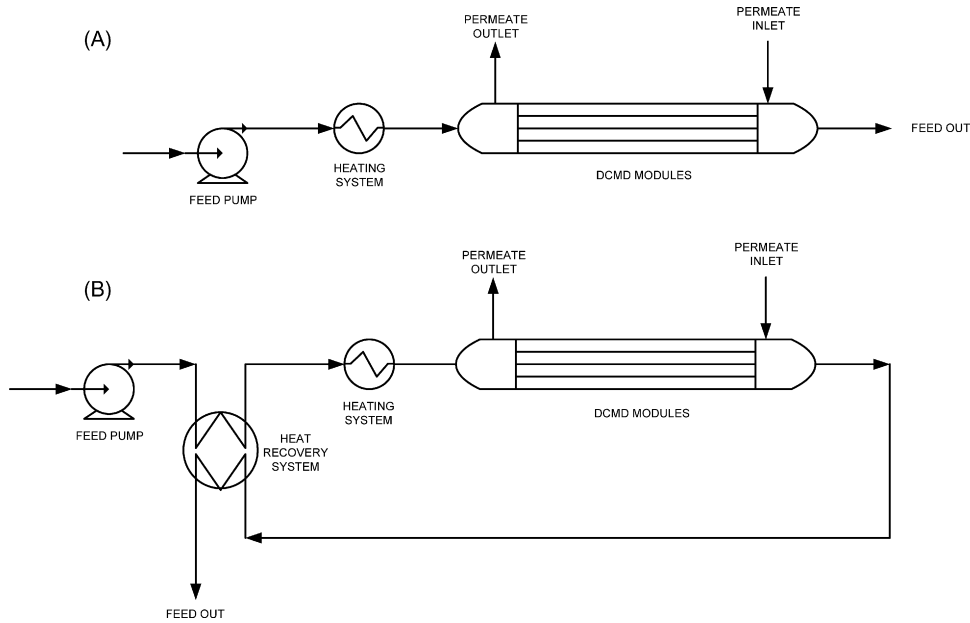
Fig. 11. Scheme of DCMD operating: (A) without heat recovery (HR) system and (B) with HR system.

The sensitivity of changing different variables of DCMD on the process economics was studied in order to identify the most sensitive parameters on total water unit cost and to establish optimal conditions for minimizing it.

An increase in the temperature difference (the driving force in membrane distillation) enhances the permeate flux per unit area, so decreasing the required membrane area and, therefore, the capital cost. On the other hand, a higher temperature difference requires more heat energy input which in turns increases the O&M costs. Consequently, an optimization between the membrane costs and the heating costs must be considered while increasing the operating temperatures of DCMD in order to obtain the best performance with minimum total unit cost of product water.

Fig. 12 shows the results of this optimization. Considering DCMD without HR, the minimum water cost was $1.23 m^{-3} obtained when operating at a feed inlet temperature of 55 °C and a temperature gradient of 25 °C. In case of DCMD with HR, the best condition was obtained when operating at a feed (inlet) temperature close to 60 °C and temperature gradient of 30 °C, with a total water cost of $1.17 m^{-3}.

In general, the water unit cost was decreasing as the DCMD water recovery factor was increased. When operating at moderate recovery factor (~50%), the difference in the water cost between DCMD with and without HR was 15%, as shown in Fig. 13. However, at high water recovery factor, the water cost of DCMD without HR became very close to the one of DCMD with HR, the difference being less than 3% at recovery ratio of
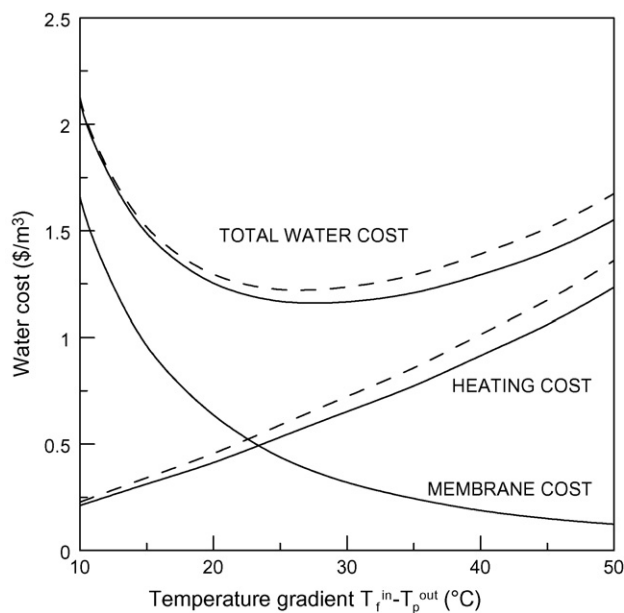
Fig. 12. Effects of temperature difference on the product water cost for DCMD without HR system (dotted line) and for DCMD with HR system (solid line).
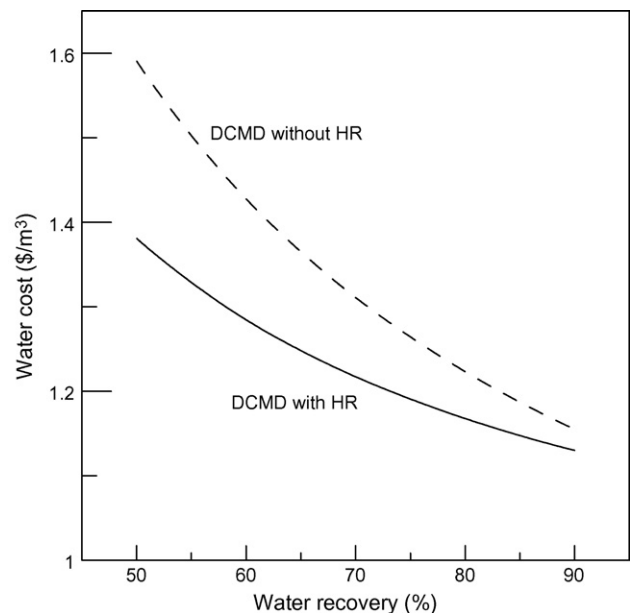
Fig. 13. Total water cost vs. water recovery for DCMD without HR system (dotted line) and for DCMD with HR system (solid line).

90%. This was due to the reduced amount of hot brine that limits the possibility to recover a significant amount of heat to be reused.

Membrane cost contributed about 50% of the total capital cost and about 30% of the O&M costs for this DCMD plant. Therefore, the cost of the product water from the MD plant was sensitive to this parameter as shown in Fig. 14. Specifically, when the cost per membrane unit area (affecting both the capital investment costs and the O&M costs since the membrane replacement was assumed as 15% of the total investment membrane cost) was increased by 10% and all other cost variables were kept constant as given in Table A.2, the total water unit cost increased by 3.9% and 3.7% in case of MD with HR and MD without HR, respectively.

In MD plant the main energy input is heat in the form of steam. The cost of energy has a wide variation among different countries and it might be even different in the same country depending on the location of the plant. As expected, the total water cost was sensitive to the specific cost of steam. As shown in Fig. 14, the total water cost increased by 4.4% and 5% for MD with and without HR system, respectively when the price of steam per ton was increased by 10% and all other cost variables were kept constant as in Table A.2.

The results of the economic analysis, tabulated in Table 4 show that the unit cost of water produced from HR-MD plant is $1.17 m^{-3}, which is 6 cent less than from MD plant without heat recovery.

This difference contributes to a total saving of $543,699 ($\sim$8%) per year in the O&M costs due to the saving in heating steam consumption (the specific heat consumption is reduced from 162 to 143 kJ/kg). The total capital cost was $1,171,253 ($\sim$4%) higher than of the MD plant without HR due to the additional costs of heat exchangers for heat recovery. However, this additional capital costs can be paid by the saving in the O&M costs within less than 2 years. The performance ratio (defined as the mass flow of the desalted water over the mass flow of the heating steam) was 12.0 in case of MD without HR, and increased to 13.7 when heat recovery system

Table 4
Cost and performance evaluation for MD with and without heat recovery (HR) system

	MD without HR	MD with HR
Total capital cost ($)	27,149,780	28,321,033
Annual fixed charge ($ m^{-3})	0.28	0.29
Membrane replacement ($/year)	2,246,256	2,246,256
Electricity ($/year)	10,515	10,515
Cost of steam ($/year)	4,580,073	4,036,374
Chemicals ($/year)	141,912	141,912
Spares ($/year)	260,172	260,172
Labor ($/year)	236,520	236,520
Brine disposal ($/year)	1,232	1,232
Total annual O&M costs ($)	7,476,680	6,932,981
Annual O&M charges ($ m^{-3})	0.95	0.88
Total water cost ($ m^{-3})	1.23	1.17
Total water cost ($ m^{-3}) when using low-grade heat energy	0.64	0.66
Performance ratio	12.0	13.7
Specific heat consumption (kJ/kg)	162	143
Primary energy (MW)	77	68

was used. The primary energy, which is the energy supplied by fuel combustion to produce thermal energy, was calculated as 77 MW in case of MD without HR and reduced by 11.7% in case of MD with HR.

Since MD requires lower operating temperatures than the conventional distillation processes, it is possible to utilize low-grade energy sources from industrial processes. This is expected to lead to significant savings in the operating costs, which in turn will result in more affordable product. Economic analysis confirms that the water cost will be as low as $0.64 m^{-3} if utilization of waste heat was considered.

In addition, MD has the potential for integration with RO in large seawater reverses osmosis plants to be operated in the brine stream. This will lead to enhancement in the process productivity by increasing the overall water recovery and reduce the environmental impact due to brine disposal. The overall recovery ratio of the integrated system based on pressure-driven membrane units (microfiltration–nanofiltration–reverse osmosis) might reach 94% if the MD is used to treat the concentrates [40].

Furthermore, small MD plants are very attractive especially if coupled with solar power to be operated in remote areas [8]. Even though the cost of water produced by this system was very high ($15 m^{-3}), it was proved that increasing the reliability of the membrane distillation technology and plant lifetime could reduce the

Fig. 14. Total water cost vs. membrane cost and steam cost (steam cost varied at a constant membrane cost of $90 m^{-2}, membrane cost varied at a constant steam cost of $7 ton^{-1}).

Table 5
Summary of estimated water cost for different literature sources

Year	Water cost ($ m^{-3})	Note	Reference
2007	1.17	MD only	This work
	0.64	MD operated using low-grade heat energy source	
2007	0.26	MD with cheap industrial waste heat	[15]
2007	0.56	NF + RO with ERD[a] and MD with available heat energy	[40]
	0.80	NF + RO without ERD[a] and MD with available heat energy	
	0.73	NF + RO with ERD[a] and MD without available heat energy	
	0.97	NF + RO without ERD[a] and MD without available heat energy	
2004	1.25	RO + MD	[4]
	1.32	MD only	

[a] ERD, energy recovery device.

cost significantly. In addition, the system was able to provide water for remote areas as a small-scale, stand-alone system with low maintenance needs.

The estimated water cost of MD plants obtained by this study was similar to the ones reported in literature recently and summarized in Table 5.

As a term of comparison, the Memstill® research group claimed to be able to obtain very competitive water cost (¢26 m^{-3}) when they operated MD using cheap industrial waste steam [15]. The water cost was between $0.56 and 0.97 m^{-3} when using MD to operate in the concentrated stream of NF and RO brine in the integrated membrane system proposed by [40].

4. Conclusions

As a thermal process, MD suffers the disadvantage of a more intensive energy requirement with respect to reverse osmosis. From this point of view, even the comparison with traditional thermal desalination systems, such as MED and MSF, seems unfavorable because of the additional resistance to mass transport and of the reduced thermal efficiency (due to heat conductivity loss) offered by the membrane. On the other hand, as an evaporative process not limited by concentration polarization, MD can operate where RO fails, showing the interesting potential to increase the water recovery factor. In addition, the high membrane area to volume ratio allows MD to operate at lower temperature with respect to traditional distillation processes, and to exploit the advantages of modularity and operational simplicity for applications in integrated membrane systems or as stand-alone small desalination units.

In order to find a reliable compromise between pros and drawbacks, this study proposes an optimization approach for DCMD not merely based on the maximization of the productivity (transmembrane flux), but also focusing on the thermal efficiency and cost.

The investigation of the complex correlations between physicochemical properties of the membrane and MD performance confirms the need for a customized hardware, i.e. high porosity hydrophobic membranes with appropriate thickness and made by low-heat conductive polymers in order to reduce the amount of waste energy.

Data from cost analysis indicate a moderate transmembrane temperature gradient (feed temperature around 60 °C) as optimal operative condition. This is an intermediate situation between athermal RO (working at around 30 °C) and high TBT (top brine temperature) seawater distillation processes (operated at around 110 °C).

Acknowledgment

Appendix A

A.1. Water vapor pressure

The dependence of water pressure from temperature is given by the Clausius–Clapeyron equation:

$$\frac{dp^0}{dT} = \frac{p^0 \lambda}{RT^2} \tag{A.1}$$

Table A.1
Values of activity of water in NaCl–H$_2$O solutions at different molality (data at 294 K) [40]

Molality (mol/kg)	a_w
1.245	0.9584
1.671	0.9438
2.200	0.9250
2.617	0.9076
3.141	0.8855
3.655	0.8635
4.086	0.8456
4.608	0.8221
5.423	0.7848

The vapor pressure of pure water is empirically given by Antoine equation [41]:

$$\ln p^0 = 23.238 - \frac{3841}{T - 45} \tag{A.2}$$

where p^0 is measured in Pa and T in K.

A.2. Water activity for aqueous NaCl solutions

Values of the activity a_w for NaCl–H$_2$O system, defined according to Eq. (A.3), were extrapolated from data of water activity a_w reported in Table A.1 [42]:

$$a_w = \frac{p^{sol}}{p^0} \tag{A.3}$$

where p^{sol} and p^0 are the vapor pressure of the NaCl–H$_2$O solution and pure water, respectively.

A.3. Economics of DCMD process

A.3.1. Data and assumption used in the economical study
See Table A.2.

Table A.2
Data and assumptions used in the economical study

Plant availability (f)	90%
Plant capacity (W)	24,000 m^3/day
Plant life	20 years
Interest rate	5%
Amortization factor (a)	0.08
Specific costs	
Electricity cost	$0.03 kWh
Membrane cost	$90 m^{-2}
Membrane replacement	15%/year
Spares cost	$0.033 m^{-3} [43]
Labor cost	$0.03 m^{-3} [44]
Chemical cost	$0.018 m^{-3} [40]
Brine disposal	$0.0015 m^{-3} [40]
Steam heat exchanger cost	$2000 m^{-2} [45]
Heat recovery exchanger cost	$1540 m^{-2} [45]

A.3.2. Sample cost calculation for a 24,000 m^3/day MD plant without HR
A.3.2.1. Operating conditions.

Feed concentration: 35 g/L
Feed seawater temperature (T_f^{sw}): 25 °C
DCMD feed inlet temperature (T_f^{in}): 55 °C
DCMD Δt: 30 °C
DCMD flux: 6.01 kg/m$_2$ h
DCMD recovery: 0.8
DCMD feed pressure: 1.2×10^5 Pa

A.3.2.2. Direct capital costs

Cost of civil work (\$) [44] = $1945(W)^{0.8} = 1945(24,000)^{0.8} = 6,209,957$

Cost of intake and pretreatment (\$) [44] = 658 (W/DCMD recovery)$^{0.8} = 658(24,000/0.8)^{0.8} = 2,511,411$

Cost of DCMD feed pumps (\$) [40] = 4.78×10^{-6} (W/DCMD recovery)$P = 4.78 \times 10^{-6} (24,000/0.8)120,000 = 17,208$

Required membrane area = $((W \times 1000/24)/N) = ((24,000 \times 1000/24)/6.01) = 166,389 \, \mathrm{m}^3$

Total cost (\$) of membrane = membrane required area × membrane cost per unit area = $166,389 \times 90 = 14,975,042$

Heat to be provided by heat exchanger $Q_{hx} = \dot{m}_f c_{pf}(T_f^{in} - T_f^{sw})/E =$ $1,250,000 \times 4184 \times (55 - 25)/0.8 = 1.96 \times 10^{11} \, \mathrm{J/h} = 54,479 \, \mathrm{kW}$; E: heat exchanger efficiency

Required heat exchanger area = $Q_{hx}/U\,\Delta T_{avg} = 54,479 \times 1000/(2500 \times 45) = 484 \, \mathrm{m}^2$; U: global heat transfer coefficient

Cost (\$) of heat exchangers = heat exchanger area × cost per $\mathrm{m}^2 = 484 \times 2000 = 968,000$

Total direct capital costs (\$) = sum of all above costs = 24,681,618.
  Indirect capital costs (\$) = 0.1 × total direct capital costs = 2,468,162.
  Total capital costs (\$) = direct costs + indirect costs = 27,149,780

Annual fixed charges = a × total capital costs
  (\$)/($f \times W \times 365$) = $0.08 \times 27,149,780/(0.9 \times 24,000 \times 365) = 0.28 \, \mathrm{m}^{-3}$

A.3.2.3. Operation and maintenance costs

Membrane replacement = 0.15 × membrane costs
  (\$/year) = 0.15 × 14,975,042 = 2,246,256

Cost of electricity (\$/year) = specific electricity cost per m^3 × annual electrical consumption = 0.03 × 350,514 = 10,515

Cost of steam (\$/year) = specific steam cost per kg × annual steam consumption = 0.007 × 654,296,130 = 4,580,073

Cost of chemicals (\$/year) = specific chemical cost per m^3 × annual plant capacity = 0.018 × 24,000 × 0.9 × 365 = 141,912

Cost of spares (\$/year) = specific spares cost per m^3 × annual plant capacity = 0.033 × 24,000 × 0.9 × 365 = 260,172

Cost of labor (\$/year) = specific labor cost per m^3 × annual plant capacity = 0.03 × 24,000 × 0.9 × 365 = 236,520

Brine disposal (\$/year) = specific brine disposal cost per m^3 × annual plant capacity = 0.015 × 24,000 × 0.9 × 365 = 1232

Total annual O&M cost (\$/year) = 7,476,680

Annual O&M charges (\$) = total annual O&M cost/annual capacity = $7,476,680/(24,000 \times 0.9 \times 365) = 0.95 \, \mathrm{m}^{-3}$

A.3.2.4. Total water cost

Total water cost (\$) = annual fixed charges + annual O&M charges = $0.27 + 0.95 = 1.23 \, \mathrm{m}^{-3}$

Nomenclature

a	polygonal cell cross-section area (mm^2)
a_f	hollow fiber cross-section area (mm^2)
$\bar{a}_f$	average hollow fiber cross-section area (mm^2)
a_0	average polygonal cell cross-section area (mm^2)
A	membrane area (m^2)
c_p	heat capacity (kJ/kg K)
$d_{m,ln}$	logarithmic mean diameter of the hollow fiber (mm)
D^k	Knudsen diffusion coefficient (m^2/s)
D^0	pressure independent molecular diffusion coefficient (Pa m^2/s)
Ex	exergy (kW)
f	friction factor
$f(\varphi)$	probability density distribution function of a polygonal cell area

h	film heat transfer coefficient (W/m^2 K)
H	overall heat transfer coefficient (W/m^2 K)
k	thermal conductivity (W/m K)
k_x	film mass transfer coefficient (m/s)
L	module length (m)
$\bar{m}$	mass flow rate (kg/s)
M	molecular weight (g/mol)
n	number of moles (mol)
N	transmembrane flux (kg/m^2 s)
N_f	number of fibers in the module
p	partial pressure (Pa)
p^0	vapor pressure (Pa)
P	total pressure (Pa)
Q	heat flux (W/m^2)
r	pore radius (μm)
R	gas constant (J/kmol K)
Re	Reynolds number
R_M	module inner radius (mm)
$R_s T_0$	entropy production (kW)
s	number of nearest neighbour fibers
T	temperature (K)
ΔT	Temperature gradient (°C)
x	molar fraction
z	axial coordinate (alongside the module) (mm)

Greek letters

δ	membrane thickness (mm)
ε	membrane porosity
η	thermal efficiency (%)
λ	heat of vaporization (kJ/kg)
ρ	density (kg/m^3)
τ	membrane tortuosity
Ξ	packing fraction probability (%)
ϕ	packing density of the hollow fiber module
ϕ_i	local packing fraction
φ	polygonal area (mm^2)
$\bar{\varphi}$	average polygonal area (mm^2)
Ψ	exergy efficiency (%)

Pedex

a	air
avg	average value
c	conduction
e	effective
f	feed side
i	ith category
id	ideal
m	across the membrane
p	permeate (distillate) side
pump	pump (in pump efficiency)
s	solid
solv	solvent
tot	total
v	vapor
w	water
0	reference status
1	interfacial at feed side
2	interfacial at permeate (distillate) side

Apex

i	ith differential element
in	inlet
out	outlet

References

[1] V. Calabrò, B.L. Jiao, E. Drioli, Theoretical and experimental study on membrane distillation in the concentration of orange juice, Industrial and Engineering Chemistry Research 33 (1994) 1803.

[2] M.S. El-Bourawi, Z. Ding, M. Khayet, A framework for better understanding membrane distillation separation process, Journal of Membrane Science 285 (2006) 4.

[3] V. Calabrò, E. Drioli, F. Matera, Membrane distillation in textile wastewater treatment, Desalination 83 (1991) 209.

[4] A.M. Alklaibi, N. Lior, Membrane-distillation desalination: status and potential, Desalination 171 (2005) 111.

[5] C. Cabassud, D. Wirth, Membrane distillation for water desalination: How to choose an appropriate membrane? Desalination 157 (2003) 307.

[6] R. Chouikh, S. Bouguecha, M. Dhahbi, Modeling of a modified air gap distillation membrane for the desalination of seawater, Desalination 181 (2005) 257.

[7] T.Y. Cath, V. Dean Adams, A.E. Childress, Experimental study of desalination using direct contact membrane distillation: a new approach to flux enhancement, Journal of Membrane Science 228 (2004) 5.

[8] F. Banat, R. Jumah, M. Garaibeh, Exploitation of solar energy collected by solar stills for desalination by membrane distillation, Renewable Energy 25 (2002) 293.

[9] Z. Ding, L. Liu, M.S. El-Bourawi, R. Ma, Analysis of a solar-powered membrane distillation system, Desalination 172 (2005) 27.

[10] J. Koschikowski, M. Wieghaus, M. Rommel, Solar thermal-driven desalination plants based on membrane distillation, Desalination 156 (2003) 295.

[11] www.scarab.se.

[12] J. Walton, H. Lu, C. Turner, S. Solis, H. Hein, Solar and Waste Heat Desalination by Membrane Distillation, 98-FC-81-0048, DWPR n. 81, El Paso, TX, April 2004.

[13] http://www.psa.es/webeng/projects/medesol/index.html.

[14] F. Banat, N. Jwaied, M. Rommel, J. Koschikowski, M. Wieghaus, Performance evaluation of the "large SMADES" autonomous desalination solar-driven membrane distillation plant in Aqaba, Jordan, Desalination 217 (2007) 17.

[15] J.H. Hanemaaijer, J. van Medevoort, A.E. Jansen, C. Dotremont, E. van Sonsbeek, Memstill membrane distillation—a future desalination, Desalination 199 (2006) 175.

[16] B. Van der Bruggen, Desalination by distillation and by reverse osmosis—trends towards the future, Membrane Technology 2 (February) (2003) 6.

[17] C. Fritzmann, J. Löwenberg, T. Wintgens, T. Melin, State-of-the-art of reverse osmosis desalination, Desalination 216 (2007) 1.

[18] http://medina.unical.it.

[19] E. Curcio, E. Drioli, Membrane distillation and related operations—a review, Separation & Purification Reviews 34 (2005) 35.

[20] K.W. Lawson, D.R. Lloyd, Membrane distillation. II. Direct contact membrane distillation, Journal of Membrane Science 120 (1996) 123.

[21] B. Li, K.K. Sirkar, Novel membrane and device for direct contact membrane distillation-based desalination processes, Industrial and Engineering Chemistry Research 43 (2004) 5300.

[22] L. Martínez-Díez, M.I. Vázquez-González, F.J. Florido-Díaz, Study of membrane distillation using channel spacers, Journal of Membrane Science 144 (1998) 45.

[23] E. Drioli, E. Curcio, A. Criscuoli, G. Di Profio, Integrated system for recovery of CaCO$_3$, NaCl and MgSO$_4$·7H$_2$O from nanofiltration retentate, Journal of Membrane Science 239 (2004) 27.

[24] A. Gabelman, S.-T. Hwang, Hollow fiber membrane contactors, Journal of Membrane Science 159 (1999) 61.

[25] J.D. Rogers, R. Long, Modeling hollow fiber membrane contactors using film theory. Voronoi tessellation and facilitation factors for systems with interface reactions, Journal of Membrane Science 134 (1997) 1.

[26] J. Wu, V. Chen, Shell-side mass transfer performance of randomly packed hollow fiber modules, Journal of Membrane Science 172 (2000) 59–74.

[27] D. Zhongwei, L. Liying, R. Ma, Study on the effect of flow maldistribution on the performance of the hollow fiber modules used in membrane distillation, Journal of Membrane Science 215 (2003) 11–23.

[28] J. Phattaranawik, R. Jiraratananon, A.G. Fane, Heat transport and membrane distillation coefficients in direct contact membrane distillation, Journal of Membrane Science 212 (2003) 177.

[29] M. Qtaishat, T. Matsuura, B. Kruczek, M. Khayet, Heat and mass transfer analysis in direct contact membrane distillation, Desalination 219 (2008) 272–292.

[30] R.H. Perry, D. Green, Perry's Chemical Engineers' Handbook, 6th edition, McGraw Hill, New York, 1984.

[31] M.F.A. Goosen, S. Sablani, H. Al-Hinai, S. Al-Obaidani, R. Al-Belushi, D. Jackson, Fouling of reverse osmosis and ultrafiltration membranes: a critical review, Separation Science and Technology 39 (2004) 2261.

[32] N. Wakao, J.M. Smith, Diffusion in catalyst pellets, Chemical Engineering Science 17 (1962) 825.

[33] N.P. Cheremisinoff, Handbook of Engineering Polymeric Materials, Dekker, New York, 1997.

[34] Y. Wu, Y. Kong, X. Lin, W. Liu, J. Xu, Surface-modified hydrophilic membranes in membrane distillation, Journal of Membrane Science 72 (1992) 189.

[35] M. Khayet, J.I. Mengual, T. Matsuura, Porous hydrophobic/hydrophilic composite membranes. Application in desalination using direct contact membrane distillation, Journal of Membrane Science 252 (2005) 101.

[36] K.W. Lawson, D.R. Lloid, Membrane distillation, Journal of Membrane Science 124 (1997) 1.

[37] A. Criscuoli, E. Drioli, Energetic and exergetic analysis of an integrated membrane desalination system, Desalination 124 (1999) 243.

[38] H. Mehdizadeh, Membrane desalination plants from an energy–exergy point of view, Desalination 191 (2006) 200.

[39] I. Dincer, M.M. Hussain, I. Al-Zaharnah, Energy and exergy use in the utility sector of Saudi Arabia, Desalination 169 (2004) 245.

[40] F. Macedonio, E. Curcio, E. Drioli, Integrated membrane systems for seawater desalination: energetic and exergetic analysis, economic evaluation, experimental study, Desalination 203 (2007) 260.

[41] R.C. Reid, J.M. Prausnitz, T.K. Sherwood, The Properties of Gases and Liquids, 3rd edition, McGraw-Hill, New York, 1977.

[42] N. Hubert, Y. Gabes, J.-B. Bourdet, L. Schuffenecker, Vapor pressure measurements with a nonisothermal static method between 293.15 and 363.15 K for electrolyte solutions. application to the H$_2$O + NaCl system, Journal of Chemical and Engineering Data 40 (1995) 891.

[43] A. Malek, M.N.A. Hawlader, J.C. Ho, Design and economics of RO desalination, Desalination 105 (1996) 245.

[44] A.M. Helal, A.M. El-Nashar, E. Al-Katheeri, S. Al-Maler, Optimal design of hybrid RO/MSF desalination plants. Part I. Modeling and algorithms, Desalination 154 (2003) 43.

[45] http://matche.com/EquipCost/Exchanger.html.